LANGMUIR

pubs.acs.org/Langmuir Article

Chemical Bath Deposition of Copper Sulfide on Functionalized SAMs: An Unusual Selectivity Mechanism

Jenny K. Hedlund, Tania G. Estrada, and Amy V. Walker*

Cite This: *Langmuir* 2020, 36, 3119−3126 Read Online

ACCESS | Metrics & More | Article Recommendations | Supporting Information

ABSTRACT: We have investigated the chemical bath deposition (CBD) of CuS using thioacetamide on functionalized self-assembled monolayers (SAMs) using scanning electron and optical microscopies, X-ray photoelectron spectroscopy, and time-of-flight secondary ion mass spectrometry. For all SAMs studied, the amount of CuS deposited is strongly dependent on the bath pH and can be attributed to the interaction of the SAM terminal groups with the chalcogenide ions present in solution. For $-CH_3$-terminated SAMs, there is a steady increase in the amount of CuS deposited with an increase in the bath pH because there is an increase in the concentration of chalcogenide ion. However, for −OH- and −COOH-terminated SAMs, we observe that the maximum amount of CuS is deposited at pH 10. We attribute this behavior to a competition between the repulsion of the chalcogenide ions by the negatively charged SAM terminal groups and an increase in the chalcogenide ion concentration with an increase in the bath pH. Using the interaction of the chalcogenide ions with the different SAM terminal functional groups, we demonstrate that CuS can be selectively deposited on the $-CH_3$-terminated areas of patterned $-OH/-CH_3$- and $-COOH/-CH_3$-terminated SAMs.

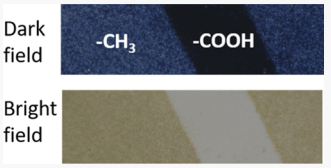

INTRODUCTION

Copper sulfide is an attractive semiconductor due to its earth abundance[1] and nontoxic qualities,[2,3] making it an attractive and low-cost option for many technological applications including in biochemistry,[4−6] photocatalysis,[7] solar cells,[2,3,8,9] and nanoelectronics.[10,11] CuS nanostructures and thin films have been fabricated by various techniques including atomic layer deposition[12] and chemical vapor deposition,[13−15] hydrothermal,[9,16−19] solvothermal,[19] microwave-assisted synthesis,[20] thermolysis,[18] spray pyrolysis,[21] sonoelectrochemical methods,[18] and chemical bath deposition (CBD).[16,22−37] CBD is an appealing method for the deposition of chalcogenide and oxide thin films. It is inexpensive, done under ambient conditions, can be performed at low temperatures (≤50 °C) which are compatible with organic thin films such as polymers, and does not require a conductive substrate.[36]

Little is known about the role of the substrate chemistry in the deposition efficiency and selectivity of CuS deposition. Chen et al.[37] and Lu et al.[16] have demonstrated that Under acidic conditions (pH ∼ 2.5), CuS is preferentially deposited on $-NH_2$-terminated self-assembled monolayers (SAMs) using almost identical bath compositions and temperature (70 °C). However, these authors come to very different conclusions about the underlying mechanism. Chen and coworkers[37] proposed that the preferential deposition occurs because there is an electrostatic interaction between the negatively charged CuS colloidal particles and the partially protonated $-NH_2$ terminal groups. In contrast, Lu and coworkers[16] indicated that the selective deposition occurs via an ion-by-ion mechanism in which the CuS layer nucleates at the Cu^{2+}−amine surface complexes.

Under basic conditions, even less is known about the CuS deposition selectivity. Previous studies have shown that the formation of surface complexes[38−41] and the hydrophobic/hydrophilic properties of the self-assembled monolayers (SAMs)[42] can be exploited to perform selective growth of ZnO,[40] ZnS,[38] CdSe,[39] and PbS.[41,42] In general, under these conditions, the interaction of the surface with the metal cation has been critical in determining the selective growth of these films. For example, the formed M^{2+}-carboxylate surface complexes, where M = Zn, Cd, and Pb, have been demonstrated to act as the nucleation sites for site-selective deposition of ZnO,[40] ZnS,[38] CdSe,[39] and PbS.[41] Finally, we note that it has also been reported that the substrate chemistry affects the properties of the deposited copper sulfide film on both organic and inorganic substrates under both acidic and basic conditions,[16,34,36,43,44] but again the mechanisms underlying these effects are not well understood.

Here, we investigate the CBD of CuS on $-CH_3$-, −OH-, and −COOH-terminated SAMs at room temperature under basic conditions using thioacetamide as a sulfur source using X-ray photoelectron spectroscopy (XPS), time-of-flight secondary ion mass spectrometry (TOF SIMS), and microscopy. We demonstrate that the deposition selectivity is strongly dependent on the interaction of the SAM terminal group with the

Received: November 4, 2019
Revised: January 7, 2020
Published: March 5, 2020

https://dx.doi.org/10.1021/acs.langmuir.9b03436
Langmuir 2020, 36, 3119−3126

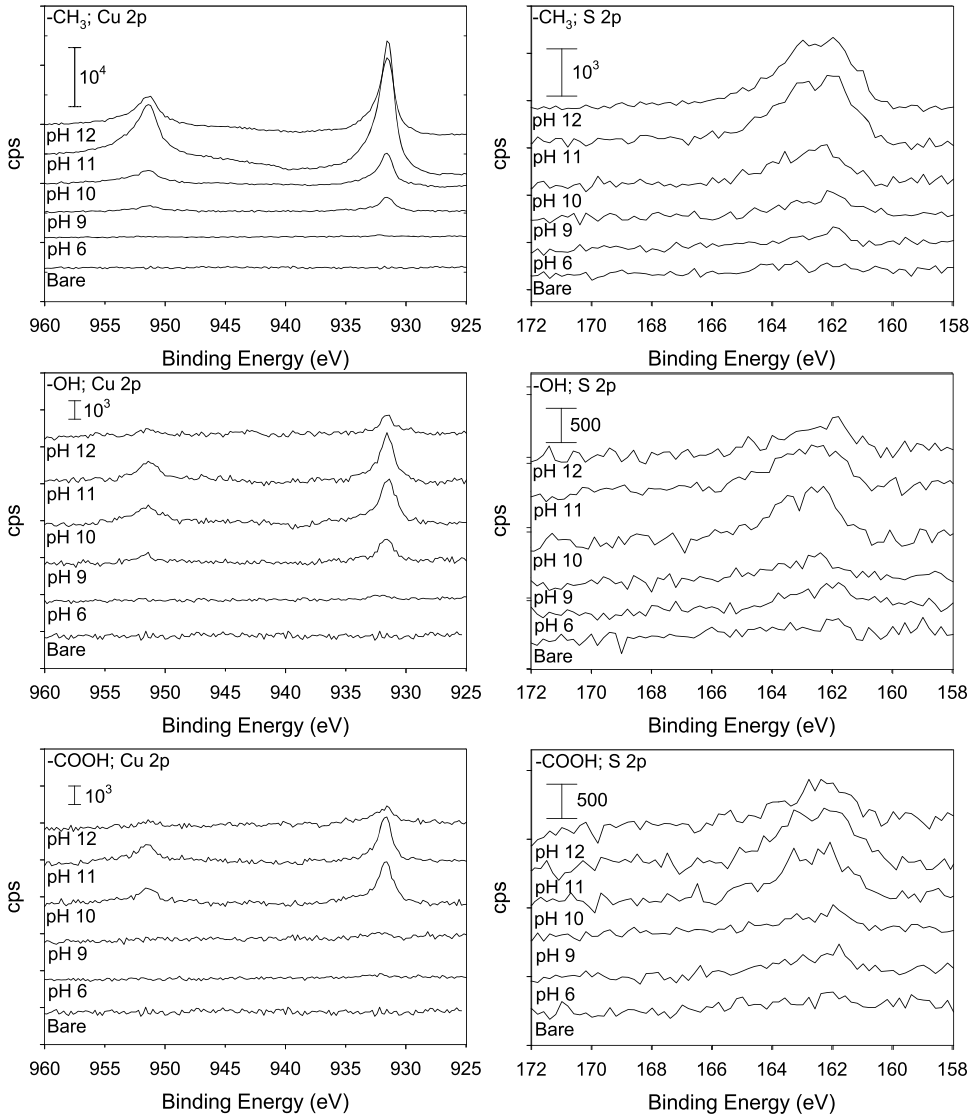

Figure 1. Variation of Cu 2p and S 2p X-ray photoelectron spectra of the CuS films deposited on $-CH_3$-, −OH-, and −COOH-terminated SAMs at bath pH for 24 h. Deposition time: 24 h. Also shown for reference are the photoelectron spectra of the bare SAMs.

sulfur-containing ions in the deposition bath. For the $-CH_3$-terminated SAMs, the amount of CuS deposited increases with an increase in the bath pH and thus the concentration of sulfur-containing ions in solution, and there is no specific interaction of the methyl terminal group with these anions. However, for −OH- and −COOH-terminated SAMs, the chalcogenide ions are repelled by the negatively charged SAM surface, which can lead to a decrease in the amount of CuS deposited as the bath pH increases. Second, we show that CuS can be selectively deposited on the $-CH_3$-terminated areas of the patterned $-OH/-CH_3$- and $-COOH/-CH_3$-terminated SAMs. In this case, selectivity is imparted by the interaction of the chalcogenide ions with the −OH- and −COOH-terminated SAMs.

EXPERIMENTAL SECTION

Materials. All of the reagents were used without further purification. Thioacetamide (99%) was obtained from Alfa Aesar, Inc. Sodium hydroxide (≥98%, pellets) was acquired from Fisher Chemicals (Thermo Fisher Scientific Inc., Waltham, MA). 16-Hydroxy-1-hexadecanethiol (99%) was purchased from Frontier Scientific Inc. (Logan, UT). 16-Mercaptohexadecanoic acid (90%), 1-hexadecanethiol (99%), ethylenediaminetetraacetic acid (98%) (EDTA), and copper(II) sulfate pentahydrate (98%) were purchased from Sigma-Aldrich Inc. (St. Louis, MO). Ethanol (200 proof, undenatured) was obtained from Spectrum Chemical MFG Corp (New Brunswick, NJ).

The gold substrates were prepared by the physical vapor deposition of ∼200 Å Cr, followed by ∼1000 Å Au on silicon wafers (⟨111⟩ orientation; Addison Engineering Inc. (San Jose, CA)) using a CHA-50 e-beam evaporator (CHA Industries, Freemont CA).

Preparation of Self-Assembled Monolayers on Gold Substrates. The preparation of alkanethiolate SAMs has been described previously.[45−47] Briefly, a well-ordered SAM was prepared by immersing a gold substrate into a 1 mM ethanolic solution of the functionalized alkanethiol (with either a $-CH_3$, $-CH_2OH$, or −COOH terminal group) for 24 h at room temperature. After removing from the alkanethiol solution, the samples were rinsed with ethanol and dried with nitrogen gas. To ensure that the SAMs were free of significant chemical contamination, the samples from each batch were analyzed by single-wavelength ellipsometry (Gaertner Scientific Corp., Skokie, IL), time-of-flight secondary ion mass spectrometry, and X-ray photoelectron spectroscopy.

Patterned $-COOH/-CH_3$- and $-OH/-CH_3$-terminated SAM substrates were prepared using photopatterning using the method of Zhou and Walker.[48] Hydroxyl or carboxylic acid terminated SAMs

https://dx.doi.org/10.1021/acs.langmuir.9b03436
Langmuir 2020, 36, 3119−3126

were exposed to UV light (500 W Hg arc lamp; Thermal Oriel-Spectra Physics Inc., Stratford CT) for 2 h through a mask. After photo-oxidation, the SAM substrate was then placed in a 1 mM ethanolic solution of hexadecanethiol for 24 h. In the photo-oxidized areas, the $-CH_3$-terminated SAM was adsorbed, leading to the formation of patterned $-COOH/-CH_3$- and $-OH/-CH_3$-terminated SAM samples.

Chemical Bath Deposition of Copper Sulfide. The deposition bath was composed of 0.006 M copper sulfate pentahydrate, 0.016 M EDTA, 0.012 M sodium hydroxide, and 0.012 M thiourea. To investigate the effect of the pH on the deposition, the bath pH was varied from pH 6 to 12. The pH of the deposition bath was adjusted using sodium hydroxide and sulfuric acid prior to the addition of the sulfur source, 0.012 M thioacetamide. The SAM substrate was immediately immersed into the bath for 24 h at room temperature. After deposition, all samples were sonicated in water for 2 min, rinsed with deionized water, dried using nitrogen gas, and stored in a nitrogen glovebox prior to further characterization.

We note that at pH 12, the bath color changed from blue to green almost immediately during deposition and became cloudy. At pH 11, the bath color also changed from blue to green over the first hour of deposition. Further, for deposition baths initially at pH 12 and 11, the solution pH decreased until it reached a pH value of 10 after 5 h. After 5 h, the bath pH remained constant at ~10. Between pH 6 and 10, the solution remained blue, and the pH did not change throughout the deposition. Photographs of the baths and pH measurements are given in the Supporting Information.

X-ray Photoelectron Spectroscopy. Ex situ XPS measurements were acquired using a PHI VersaProbe II (Physical Electronics Inc., Chanhassen, MN) with an Al Kα source (E_b = 1486.7 eV). During data collection, the chamber pressure was maintained at $<5 \times 10^{-10}$ mbar. High-resolution photoelectron spectra were collected with a pass energy of 23.5 eV, an energy step of 0.2 eV, and an analysis angle of 45°. All spectra were obtained using a charge compensation with both electron and ion beams incident on the surface. The binding energies were calibrated to the Au $4f_{7/2}$ binding energy (84.0 eV).

The data were analyzed using CasaXPS 2.3.17 (RBD Instruments, Inc., Bend OR). The Cu $2p_{3/2}$ peak height was obtained in the following way. The Cu 2p spectra were fit with a Shirley background. The peak height was obtained from the difference between the number of counts at the Cu $2p_{3/2}$ photoelectron peak maximum and the Shirley background intensity.

All XPS measurements were performed within 24 h of CuS CBD, and at least three samples were prepared (on different days) with three areas analyzed for each deposition condition. The spectra shown are representative of the data obtained.

Time-of-Flight Secondary Ion Mass Spectrometry. The TOF SIMS data were collected with an ION TOF IV (ION TOF Inc., Chestnut Hill, NY) equipped with a Bi liquid metal ion gun. The instrument comprised of three chambers: a loadlock, a preparation chamber, and an analysis chamber. During data collection, the pressure of the analysis chamber was kept at $<5 \times 10^{-9}$ mbar. The Bi^+ primary ions had a kinetic energy of 25 keV and were contained in a ~100 nm probe beam. All of the spectra were acquired using an analysis area of 100 × 100 μm^2 and within the static regime using a total ion dose of less than 10^{10} ions cm^{-2}.

For each experimental condition, at least three samples were prepared (on different days), and three areas on each sample were examined. The spectra shown are characteristic of these data.

Optical and Secondary Electron Microscopy. Scanning electron microscopy (SEM) and optical microscopy were employed to image the deposits. SEM measurements were acquired on a Supra-40 scanning electron microscope (Zeiss), while optical microscopy was performed using a Keyence VHX-2000 digital microscope. The images shown are representative of the data obtained.

RESULTS AND DISCUSSION

Figure 1 displays the Cu 2p and S 2p X-ray photoelectron spectra of the deposited CuS films after 24 h using deposition baths with varying pH values. For every deposition bath pH and functionalized SAM, the Cu $2p_{3/2}$ and Cu $2p_{1/2}$ binding energies are 931.9 ± 0.3 eV and 951.6 ± 0.2 eV, indicating that CuS has been deposited (see Supporting Information Table S1).[49−51] The modified Auger parameter, which is the sum of the Cu $2p_{3/2}$ binding energy and Cu LMM kinetic energy, is 1850.2 ± 0.3 eV, also consistent with the formation of CuS (see Supporting Information Table S1).[49,51] Although the S 2p photoelectron peak cannot be resolved into $2p_{3/2}$ and $2p_{1/2}$ peaks, the S 2p binding energy, ~162.5 eV, is also consistent with the deposition of CuS.[49,50] Further, full width at half-maximum (FWHM) of the S 2p peak is ~2.6 eV, which is much larger than that of ~1.5 eV of the Cu 2p photoelectron peaks.[50] This suggests that the S 2p photoelectron peak is composed of two doublets of the S^{2-} and S_2^{2-} ligands present in CuS.[50] Finally, consistent with the deposition of CuS, the calculated ratio of the S/Cu concentration is equal to the expected stoichiometry of 1.0 within the experimental error (see Supporting Information Table S1).

The C 1s photoelectron spectra indicate that there is no interaction between the SAM and deposited CuS. No new photoelectron peaks are observed in the spectra. However, upon CuS CBD, the intensities of the C 1s and O 1s photoelectron peaks increase, and their binding energies increase and then decrease. This is likely due to charge transfer between the CuS and gold substrate, which is mediated by the dipole of the functionalized SAM (see Supporting Information Figures S5 and S6). Similar effects have been observed by Jiang et al.[52] for the Au clusters deposited on rutile.

The XPS data also show that the amount of CuS deposited is dependent on both the bath pH and the identity of the SAM functional group (Figure 1). Figure 2 displays the variation of

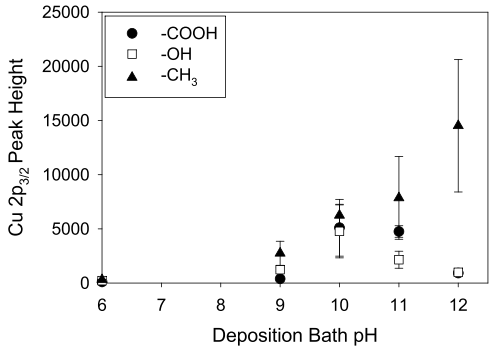

Figure 2. Variation of the Cu $2p_{3/2}$ photoelectron peak height with bath pH after CBD of CuS on $-COOH$-, $-OH$-, and $-CH_3$-terminated SAMs for 24 h at room temperature.

the Cu $2p_{3/2}$ photoelectron peak height with bath pH after deposition on $-CH_3$-, $-OH$-, and $-COOH$-terminated SAMs for 24 h at room temperature. The Cu $2p_{3/2}$ peak height can be used here as a quantitative measure of the amount of CuS deposited because it is related to the peak area and there are no overlapping peaks or interferences in the photoelectron spectra, which would lead to inaccuracies in the quantitative estimation. Further, the XPS data are consistent with the CuS film thicknesses measured using AFM (after sonication). At pH 12, the adherent CuS film is ~50 nm thick, at pH 11 ~35 nm, and at pH 10 ~8 nm. In general, the Cu $2p_{3/2}$ peak height increases with an increase in bath pH, indicating that more CuS has been deposited. However for $-OH$- and $-COOH$-

https://dx.doi.org/10.1021/acs.langmuir.9b03436
Langmuir 2020, 36, 3119−3126

terminated SAMs, the amount of CuS decreases, as evidenced by the Cu $2p_{3/2}$ peak height, for bath pH ≥ 11. In contrast, on $-CH_3$-terminated SAMs, the amount of CuS increases with increasing bath pH. We note that at pH 11 and 12, the error bars significantly increase, suggesting that the deposited layer has become rough or is nonuniform.

We also observed differences in the growth of the CuS layer with deposition time. Figure 3 displays the variation of the Cu

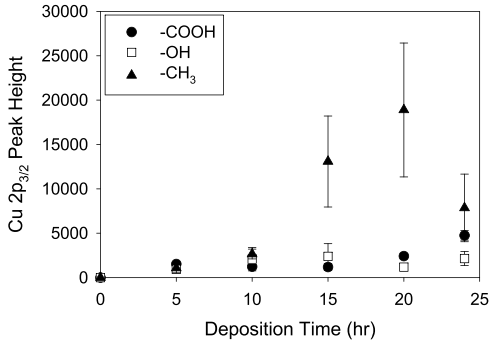

Figure 3. Variation of the Cu $2p_{3/2}$ peak height with deposition time after CBD of CuS on −COOH-, −OH-, and $-CH_3$-terminated SAMs at pH 11 and room temperature.

$2p_{3/2}$ peak height with deposition time at pH 11. For $-CH_3$-terminated SAMs, the amount of CuS deposited initially increases slowly and then quickly increases after the deposition time of 10 h. It is interesting to note that the faster growth occurs after the deposition bath pH has reached its equilibrium value pH of ∼10 (see the Supporting Information). The amount of CuS deposited appears to reach a plateau after 15 h. Between 15 and 24 h, we note that there is a wider variation in the Cu $2p_{3/2}$ height, suggesting that the deposit is either rough or nonuniform. In contrast, for −OH- and −COOH-terminated SAMs, a much smaller amount of CuS is deposited, as measured by the Cu $2p_{3/2}$ peak height. Initially, the Cu $2p_{3/2}$ peak height increases slowly until it reaches a plateau after 5 h of deposition and then starts to increase after ∼20 h deposition time.

The TOF SIMS measurements are in agreement with the XPS data. For all experimental conditions and functionalized SAMs studied, $Cu_xS_yH_z^{\pm}$ ions are observed in the positive and negative ion mass spectra, indicating that CuS has been deposited. Further, the data show that the SAM molecular cluster ion intensities, Au_2M^- and AuM_2^- (where M = $-S(CH_2)_{15}CH_3$, $-S(CH_2)_{15}CH_2OH$, or $-S(CH_2)_{15}COOH$), also decrease with decrease in bath pH, indicating that the functionalized SAMs are increasingly covered by the deposited CuS layer (Figure 4). This observation suggests that more CuS is deposited as the bath pH increases. For all SAMs studied for depositions at pH > 11, no molecular cluster ions are observed, indicating that the CuS layer has fully covered the substrate. Additionally, for −COOH-terminated SAMs at bath pH ≥ 9, we observe that ions are of the form $CuCOO(CH_2)_x(CH)_y^+$, indicating that Cu^{2+} ions interact with the −COOH terminal group (Figure 5) and are characteristic of the formation of copper-carboxylate complexes.[53,54]

Reaction Pathways. The reaction pathways involved in the CBD of CuS on functionalized SAMs using thioacetamide must account for the following observations:

(a) At pH 6, very little copper sulfide is deposited.

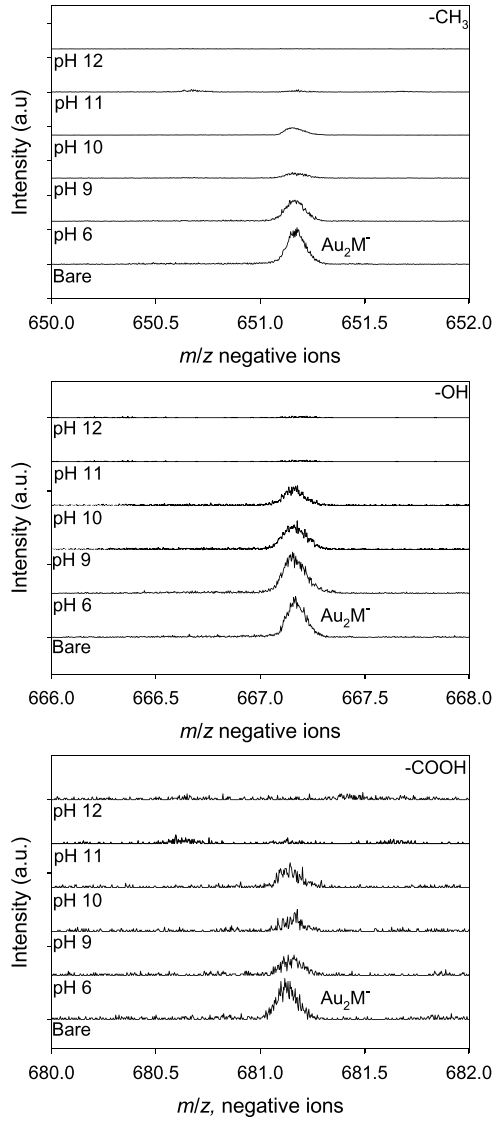

Figure 4. High-resolution negative-ion spectra of Au_2M^- after the deposition of copper sulfide on $-CH_3$-, −OH-, and −COOH-terminated SAMs, where M = $-S(CH_2)_{15}CH_3$, $-S(CH_2)_{15}CH_2OH$, and $-S(CH_2)_{15}COOH$, respectively, for 24 h at room temperature. The deposition bath pH was varied from pH 6 to 12. Also shown for reference are the mass spectra of the bare SAMs.

(b) The largest amount of copper sulfide is deposited on $-CH_3$-terminated SAMs.

(c) At pH 11, the largest amount of CuS is deposited on −OH- and −COOH-terminated SAMs.

(d) There is a steady increase in the amount of CuS deposited on $-CH_3$-terminated SAMs as the bath pH increases.

(e) The nucleation time for CuS deposition on $-CH_3$-terminated SAMs is slightly faster than that for CuS deposition on −OH- and −COOH-terminated SAMs.

In CBD reactions, the concentration of the metal ion and the chalcogenide ion are controlled.[36] Under basic reaction conditions, CuS can be deposited using the following (unbalanced) reaction pathway (chemical reaction)[36,55]

$$Cu^{2+} + EDTA^{4-} \rightarrow [Cu(EDTA)]^{2-} \quad (1)$$

$$CH_3CSNH_2 + 2OH^- \rightarrow CH_3COO^- + NH_3 + HS^- \quad (2)$$

https://dx.doi.org/10.1021/acs.langmuir.9b03436
Langmuir 2020, 36, 3119−3126

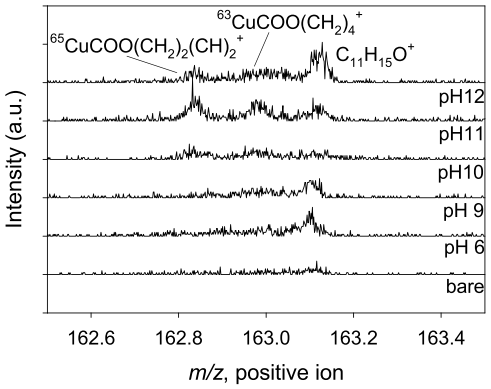

Figure 5. High-resolution positive-ion spectra centered at m/z 163 after the deposition of CuS on −COOH-terminated SAMs for 24 h at room temperature. The deposition bath pH was varied from pH 6 to 12. Also shown for reference are the mass spectra of the bare SAMs.

$$HS^- + OH^- \rightarrow S^{2-} + H_2O \quad (3)$$

$$Cu^{2+} + S^{2-} \rightarrow CuS \quad (4)$$

The concentration of "free" copper ions is controlled by a complexing agent, ethylenediaminetetraacetic acid (EDTA) (reaction 1). Thioacetamide reacts with hydroxide ions present in a solution to form bisulfide ions, HS^- (reaction 2). Subsequently, the bisulfide ions decompose to S^{2-} ions (reaction 3), which then react with Cu^{2+} ions to form CuS (reaction 4). However, in weakly acidic solutions (i.e., pH 6), the deposition reaction may proceed through the decomposition of a Cu^{2+}−thioacetamide complex rather than the formation of an intermediate bisulfide and sulfide ion.[36] This reaction is much slower than the hydrolysis of thioacetamide under basic conditions (reactions 2 and 3), and so less copper sulfide is deposited at pH 6 than at higher pH. Reactions 2 and 3 also clearly show that as the bath pH increases, i.e., the concentration of OH^- ions in the bath increases, the deposition rate is likely to increase. This is because, by Le Chatelier's principle, the increased $[OH^-]$ concentration will drive reactions 2 and 3 to the product side leading to an increase in the S^{2-} concentration and deposition of more CuS (reaction 4).

The deposition on functionalized SAMs can proceed via an ion-by-ion growth in which deposition occurs via successive cation−anion absorption on the growing deposit and/or by a cluster-by-cluster growth in which there is the formation of colloidal particles in solution, followed by aggregation and their deposition on the substrate.[36] Thus, the placement and deposition of films synthesized using ion-by-ion growth are strongly dependent on the substrate chemistry.[38−41] Further, deposits formed by cluster-by-cluster growth do not strongly adhere to the substrate. To investigate the effect of the functionalized SAMs on CuS CBD, we therefore thoroughly rinsed and sonicated the samples before analysis so that only CuS films deposited using ion-by-ion growth were investigated.

Our experiments clearly indicate that the reaction pathways involved in CuS CBD are more complicated than the above discussion suggests. It is likely that at pH 12, there are other copper complexes present in the deposition bath because the solution changes from blue to green, and so the deposition pathways are altered. The data also clearly show that the chemical nature of the SAM terminal group is also important in the deposition process. Methyl-terminated SAMs are hydrophobic, while hydroxyl and carboxylic acid terminated SAMs are hydrophilic. However, this cannot account for the deposition differences observed. If the hydrophobicity/hydrophilicity of the substrates controlled the CBD process, we would expect that the least amount of CuS would be deposited on the $-CH_3$-terminated SAMs at every bath pH studied. However, at pH ≥ 9, more copper sulfide is deposited on the hydrophobic $-CH_3$-terminated SAM than that on the −COOH- and −OH-terminated SAMs (Figures 1 and 2). This indicates that it is the interaction of the precursor ions with the SAM terminal groups that leads to the differences in the observed deposition.

We propose that the deposition can be explained via a kinetically controlled reaction. For $-CH_3$-terminated SAMs, the terminal C−H bonds are nonpolar. Consequently, there is no specific interaction between either the Cu^{2+} or S^{2-} ions in solution and the $-CH_3$ terminal group. Nucleation of the copper sulfide layer likely occurs due to trapping (most likely at defects) of either Cu^{2+} or S^{2-} ions or by the precipitation of small clusters (cluster-by-cluster growth).[38−41,55] As the pH of the deposition bath increases, there is a steady increase in the amount of copper sulfide deposited because the concentration of S^{2-} in solution increases. In contrast, hydroxyl-terminated SAMs have a polar terminal C−OH bond, which has a dipole oriented such that the −OH group has a small negative charge (δ^-). As the deposition bath pH increases above 10, the negatively charged −OH group repels some of the S^{2-} ions and other anions in solution, leading to less CuS deposited than that on $-CH_3$-terminated SAMs and a decrease in the overall amount of CuS deposited (Figure 3).

For −COOH-terminated SAMs, the data suggest that there are two competing effects. For −COOH-terminated SAMs, the surface $pK_{1/2}$ is ∼8.0, which is the pH of the solution at which the surface is 50% ionized.[56] Thus, as the bath pH increases, the −COOH terminal group deprotonates to form carboxylate ions, COO^-, and at pH 12, the surface is almost fully deprotonated. This leads to the formation of copper-carboxylate complexes, which serve as the nucleation sites for subsequent deposition (Figure 5).[38−41,53,54] However, at pH 12, the amount of copper sulfide decreases significantly (Figure 3). The equilibrium constant, K, for the complexation of Cu^{2+} and carboxylic acids (<100)[57] is very low. In the deposition bath, there is a large concentration of EDTA and Cu^{2+} has a very high binding constant to EDTA (5×10^{18});[58] therefore, it is likely that few copper complexes will be formed. This suggests that as the pH increases and becomes more negatively charged, there is a competition between the nucleation of the CuS layer at the Cu-carboxylate surface complexes and the repulsion between the negatively charged COO^- functionalized surface and sulfur ions present in the solution. Thus, at pH 11, more CuS is deposited on the −COOH-terminated SAMs than on the −OH-terminated SAMs due to the formation of copper-carboxylate complexes. However, at pH 12, the repulsion between the negatively charged sulfur ions in the solution and the negatively charged surface dominate the CBD process, leading to a decrease in the amount of CuS deposited.

Selective Deposition of CuS. These results indicate that under appropriate conditions, CBD can be employed to selectively deposit CuS without the formation of metal-surface complexes. Rather, the different deposition and nucleation rates for $-CH_3$-, −OH-, and −COOH-terminated SAMs can be employed to selectively deposit CuS on $-CH_3$-terminated

https://dx.doi.org/10.1021/acs.langmuir.9b03436
Langmuir 2020, 36, 3119−3126

SAMs. Here, the selectivity is imparted by the different interactions of the produced bisulfide and sulfur ions with the $-CH_3$-, −OH-, and −COOH-terminated SAMs. In Figure 6,

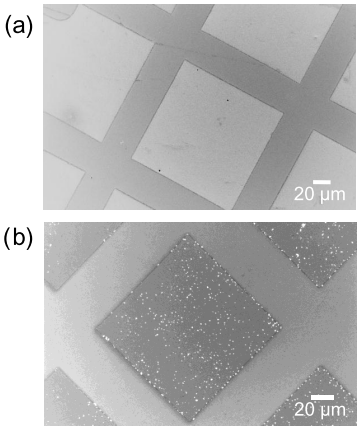

Figure 6. SEM images of CuS deposited at pH 11 (a) on a patterned $-CH_3$/−COOH-terminated SAM for 11 h and (b) on a patterned $-CH_3$/−OH-terminated SAM for 19 h.

the SEM images indicate that CuS has been deposited only on the $-CH_3$-terminated SAM region ("square" areas) after CBD of CuS on $-CH_3$/−OH- or $-CH_3$/−COOH-terminated patterned SAMs. In the "bar" areas, which are composed of either −OH- or −COOH-terminated SAMs no crystallites or deposits are observed.

CONCLUSIONS

CBD of copper sulfide using thioacetamide is strongly dependent on the interaction of the precursors, in particular the sulfur-containing ions, with the chemical identity of the SAM functional groups. For $-CH_3$-terminated SAMs, there is no specific interaction with the deposition bath reagents. As the bath pH increases, there is a steady increase in the amount of CuS deposited due to an increase in the concentration of sulfur-containing ions in the bath. For −OH-terminated SAMs, there is an initial increase in the CuS deposited with an increase in bath pH, which can also be attributed to the increase in the sulfur-containing ion concentration. However, above pH 10, the amount of CuS decreases and is less than that on $-CH_3$-terminated SAMs because the chalcogenide ions in a solution are repelled by a slightly negatively charged, polar −OH terminal group.

For −COOH-terminated SAMs, there are two competing effects: the formation of copper-carboxylate surface complexes, which can serve as the nucleation sites for film growth, and the repulsion of S^{2-} ions by the negatively charged $-COO^-$-terminated surface. Thus, at pH 10 and 11, more copper sulfide is deposited on −COOH-terminated SAMs due to the formation of surface copper-carboxylate complexes, which serve as nucleation sites for CuS deposition. At pH 12, similar amounts of CuS are deposited on −OH- and −COOH-terminated SAMs due to the repulsion of the negatively charged sulfur-containing ions by the negatively charged SAM surface.

These experiments indicate that there is a second method to successfully perform selective CBD of inorganic chalcogenides on organic surfaces. Rather than exploiting the formation of metal-surface complexes, the interaction of chalcogenide ion with different functional groups can be employed to manipulate the selectivity of the deposition. Further, the interaction of the chalcogenide ion with the surface functional group can lead to selective deposition even if metal-surface complexes are present.

ASSOCIATED CONTENT

Supporting Information

The Supporting Information is available free of charge at https://pubs.acs.org/doi/10.1021/acs.langmuir.9b03436.

Variation of bath pH with time and color of the deposition bath; XPS characterization of the precipitates; variation of the binding energy of Cu $2p_{3/2}$, kinetic energy of Cu LMM, modified Auger parameter (α'), and ratio of S to Cu determined by XPS with bath pH for CuS films deposited on −COOH-, −OH-, and $-CH_3$-terminated SAMs; C 1s and O 1s photoelectron spectra of X-ray photoelectron spectra of CuS films deposited on $-CH_3$-, −OH-, and −COOH-terminated SAMs at bath pH for 24 h (PDF)

AUTHOR INFORMATION

Corresponding Author

Amy V. Walker − *Department of Chemistry and Biochemistry and Department of Materials Science and Engineering, University of Texas at Dallas, Richardson, Texas 75080, United States;* orcid.org/0000-0003-2114-3644; Phone: +1 972 883 5780; Email: amy.walker@utdallas.edu; Fax: +1 972 883 5725

Authors

Jenny K. Hedlund − *Department of Chemistry and Biochemistry, University of Texas at Dallas, Richardson, Texas 75080, United States;* orcid.org/0000-0001-8569-802X

Tania G. Estrada − *Department of Chemistry and Biochemistry, University of Texas at Dallas, Richardson, Texas 75080, United States*

Complete contact information is available at: https://pubs.acs.org/10.1021/acs.langmuir.9b03436

Author Contributions

The manuscript was written through contributions of all authors.

Notes

The authors declare no competing financial interest.

ACKNOWLEDGMENTS

The authors gratefully acknowledge support from the National Science Foundation (CHE 1708258) and Rohan Joshi for his help with preliminary experiments on CBD of CuS.

ABBREVIATIONS USED

CBD, chemical bath deposition; SAM, self-assembled monolayer; EDTA, ethylenediaminetetraacetic acid; XPS, X-ray photoelectron spectroscopy; TOF SIMS, time-of-flight secondary ion mass spectrometry; FWHM, full width at half-maximum

REFERENCES

(1) Rare Earth Elements-Critical Resources for High Technology. https://pubs.usgs.gov/fs/2002/fs087-02 (accessed Nov 23, 2018).

https://dx.doi.org/10.1021/acs.langmuir.9b03436
Langmuir 2020, 36, 3119−3126

(2) Shah, A.; Torres, P.; Tscharner, R.; Wyrsch, N.; Keppner, H. Photovoltaic Technology: The Case for Thin-Film Solar Cells. *Science* **1999**, *285*, 692−698.
(3) Polman, A.; Knight, M.; Garnett, E. C.; Ehrler, B.; Sinke, W. C. Photovoltaic materials: Present efficienies and future challenges. *Science* **2016**, *352*, No. aad4424.
(4) Bai, J.; Jiang, X. A Facile One-Pot Synthesis of Copper Sulfide-Decorated Reduced Graphene Oxide Composites for Enhanced Detecting of H_2O_2 in Biological Environments. *Anal. Chem.* **2013**, *85*, 8095−8101.
(5) Ding, K.; Zeng, J.; Jing, L.; Qiao, R.; Liu, C.; Jiao, M.; Li, Z.; Gao, M. Aqueous synthesisi of PEGylated copper sulfide nanoparticles for photoacoustic imaging of tumors. *Nanoscale* **2015**, *7*, 11075−11081.
(6) Goel, S.; Chen, F.; Cai, W. Synthesis and Biomedical Applications of Copper Sulfide Nanoparticles: From Sensors to Theranostics. *Small* **2014**, *10*, 631−645.
(7) Chen, X.; Li, H.; Wu, Y.; Wu, H.; Wu, L.; Tan, P.; Pan, J.; Xiong, X. Facile fabrication of novel porous graphitic carbon nitride/copper sulfide nanocomposites with enhanded visible light driven photocatalytic performance. *J. Colloid Interface Sci.* **2016**, *476*, 132−143.
(8) Lee, H.; Yoon, S. W.; Kim, E. J.; Park, J. In-Situ Growth of Copper Sulfide Nanocrystals on Multiwalled Carbon Nanotubes and Their Application as Novel Solar Cell and Amperometric Glucose Sensor Materials. *Nano Lett.* **2007**, *7*, 778−784.
(9) Wu, Y.; Wadia, C.; Ma, W.; Sadtler, B.; Alivisatos, A. P. Synthesis and Photovoltaic Application of Copper(I) Sulfide Nanocrystals. *Nano Lett.* **2008**, *8*, 2551−2555.
(10) Sakamoto, T.; Sunamura, H.; Kawaura, H.; Hasegawa, T.; Nakayama, T.; Aono, M. Nanometer-scale switches using copper sulfide. *Appl. Phys. Lett.* **2003**, *82*, 3032−3034.
(11) Tang, J.; Huo, Z.; Brittman, S.; Gao, H.; Yang, P. Solution-processed core-shell nanowires for efficient photovoltaic cells. *Nat. Nanotechnol.* **2011**, *6*, 568−572.
(12) Martinson, A. B. F.; Riha, S. C.; Thimsen, E.; Elam, J. W.; Pellin, M. J. Structural, optical, and electronic stability of copper sulfide thin films grown by atomic layer deposition. *Energy Environ. Sci.* **2013**, *6*, 1868−1878.
(13) Carbone, I.; Zhou, Q.; Vollbrecht, B.; Yang, L.; Medling, S.; Bezryadina, A.; Bridges, F.; Aler, G. B.; et al. Pulsed chemical vapor deposition of Cu_2S into a porous TiO_2 matrix. *J. Vac. Sci. Technol., A* **2011**, *29*, No. 051505.
(14) Nomura, R.; Miyawaki, K.; Toyosaki, T.; Matsuda, H. Preparation of Copper Sulfide Thin Layers by a Single-Source MOCVD Process. *Chem. Vap. Deposition* **1996**, *2*, 174−179.
(15) Abdelhady, A. L.; Ramasamy, K.; Malik, M. A.; O'Brien, P.; Haigh, S. J.; Raftery, J. New routes to copper sulfide nanostructures and thin films. *J. Mater. Chem.* **2011**, *21*, 17888−17895.
(16) Lu, Y.; Meng, X.; Yi, G.; Jia, J. In situ growth of CuS thin films on functionalized self-assembled monolayers using chemical bath deposition. *J. Colloid Interface Sci.* **2011**, *356*, 726−733.
(17) Chen, X.; Wang, Z.; Wang, X.; Zhang, R.; Liu, X.; Lin, W.; Qian, Y. Synthesis of novel copper sulfide hollow spheres generated from copper (II)-thiourea complex. *J. Cryst. Growth* **2004**, *263*, 570−574.
(18) Zhao, Y.; Pan, H.; Lou, Y.; Qiu, X.; Zhu, J.; Burda, C. Plasmonic $Cu_{2-x}S$ Nanocrystals: Optical and Structural Properties of Copper-Deficient Copper(I) Sulfides. *J. Am. Chem. Soc.* **2009**, *131*, 4253−4261.
(19) Shamraiz, U.; Hussain, R. A.; Badshah, A. Fabrication and applications of copper sulfide (CuS) nanostructures. *J. Solid State Chem.* **2016**, *238*, 25−40.
(20) Liao, X.-H.; Chen, N.-Y.; Xu, S.; Yang, S.-B.; Zhu, J.-J. A microwave assisted heating method for the preparation of copper sulfide nanorods. *J. Cryst. Growth* **2003**, *252*, 593−598.
(21) Isac, L.; Duta, A.; Kriza, A.; Manolache, S.; Nanu, M. Copper sulfides obtained by spray pyrolysis - Possible absorbers in solid-state solar cells. *Thin Solid Films* **2007**, *515*, 5755−5758.
(22) Nair, M. T. S.; Nair, P. K. Chemical bath deposition of Cu_xS thin films and their prospective large area applications. *Semicond. Sci. Technol.* **1989**, *4*, 191−199.
(23) Vas-Umnuay, P.; Chang, C.-h. Growth Kinetics of Copper Sulfide Thin Films by Chemical Bath Deposition. *ECS J. Solid State Sci. Technol.* **2013**, *2*, P120−P129.
(24) Lindroos, S.; Arnold, A.; LeskelÃ, M. Growth of CuS thin films by the successive ionic layer adsorption and reaction method. *Appl. Surf. Sci.* **2000**, *158*, 75−80.
(25) Lokhande, C. D. A chemical method for preparation of metal sulfide thin films. *Mater. Chem. Phys.* **1991**, *28*, 145−149.
(26) Gadave, K. M.; Lokhande, C. D. Formation of Cu_xS films through a chemical bath deposition process. *Thin Solid Films* **1993**, *229*, 1−4.
(27) Munce, C. G.; Parker, G. K.; Holt, S. A.; Hope, G. A. A Raman spectroelectrochemical investigation of chemical bath deposited CuxS thin films and their modification. *Colloids Surf., A* **2007**, *295*, 152−158.
(28) Fatas, E.; Garcia, T.; Montemayor, C.; Medina, A.; Camarero, E. G.; Arjona, F. Formation of Cu_xS thin films through a chemical bath deposition process. *Mater. Chem. Phys.* **1985**, *12*, 121−128.
(29) Fernandez, A. M.; Sebastian, P. J.; Campos, J.; Gomez-Daza, O.; Nair, P. K.; Nair, M. T. S. Structural and opto-electronic properties of chemically deposited CuxS thin film and the precipitate. *Thin Solid Films* **1994**, *237*, 141−147.
(30) Grozdanov, I.; Barlingay, C. K.; Dey, S. K. Novel applications of chemically deposited Cu_xS thin films. *Mater. Lett.* **1995**, *23*, 181−185.
(31) Grozdanov, I.; Najdoski, M. Optical and Electrical Properties of Copper Sulfide Films of Variable Composition. *J. Solid State Chem.* **1995**, *114*, 469−475.
(32) Huang, L.; Zingaro, R. A.; Meyers, E. A.; Nair, P. K.; Nair, M. T. S. Chemical Deposition of Thin Films of Copper Sulfide on Glass Surfaces Modified with Organosilanes. *Phosphorus, Sulfur Silicon Relat. Elem.* **1995**, *105*, 175−185.
(33) Nair, M. T. S.; Guerrero, L.; Nair, P. K. Conversion of chemically deposited CuS thin films to $Cu_{1.8}S$ and $Cu_{1.96}S$ by annealing. *Semicond. Sci. Technol.* **1998**, *13*, 1164.
(34) Nair, P. K.; Nair, M. T. S.; Pathirana, H. M. K. K.; Zingaro, R. A.; Meyers, E. A.; et al. Structure and Composition of Chemically Deposited Thin Films of Bismuth Sulfide and Copper Sulfide: Effect on Optical and Electrical Properties. *J. Electrochem. Soc.* **1993**, *140*, 754−759.
(35) Sagade, A. A.; Sharma, R. Copper sulphide (CuxS) as an ammonia gas sensor working at room temperature. *Sens. Actuators, B* **2008**, *133*, 135−143.
(36) Hodes, G. *Chemical Solution Deposition of Semiconductor Films*; Marcel Dekker Inc.: New York, 2002.
(37) Chen, M.; Zhao, J.; Zhao, X. Scanning electrochemical microscopy studies of micropatterned copper sulfide (CuxS) thin films fabricated by a wet chemistry method. *Electrochim. Acta* **2011**, *56*, 5016−5021.
(38) Lu, P.; Walker, A. V. Making Nanoflowerbeds: Reaction Pathways Involved in the Selective Chemical Bath Deposition of ZnS on Functionalized Alkanethiolate Self-Assembled Monolayers. *ACS Nano* **2009**, *3*, 370−378.
(39) Lu, P.; Walker, A. V.; et al. Selective Formation of Monodisperse CdSe Nanoparticles on Functionalized Self-Assembled Monolayers Using Chemical Bath Deposition. *Electrochim. Acta* **2010**, *55*, 8126−8134.
(40) Shi, Z.; Walker, A. V. Chemical Bath Deposition of ZnO on Functionalized Self-Assembled Monolayers: Selective Deposition and Control of Deposit Morphology. *Langmuir* **2015**, *31*, 1421−1428.
(41) Yang, J.; Walker, A. V. Morphological Control of PbS Grown on Functionalized Self-Assembled Monolayers by Chemical Bath Deposition. *Langmuir* **2014**, *30*, 6954−6962.
(42) Meldrum, F. C.; Flath, J.; Knoll, W. Formation of Patterned PbS and ZnS Films on Self-Assembled Monolayers. *Thin Solid Films* **1999**, *348*, 188−195.

https://dx.doi.org/10.1021/acs.langmuir.9b03436
Langmuir 2020, 36, 3119−3126

(43) Safrani, T.; Jopp, J.; Golan, Y. A comparative study of the structure and optical properties of copper sulfide thin films chemically deposited on various substrates. *RSC Adv.* **2013**, *3*, 23066−23074.
(44) Yamamoto, T.; Tanaka, K.; Kubota, E.; Osakada, K. Deposition of copper sulfide on the surface of poly(ethylene terephthalate) and poly(vinyl alcohol) films in aqueous solution to give electrically conductive films. *Chem. Mater.* **1993**, *5*, 1352−1357.
(45) Fisher, G. L.; Walker, A. V.; Hooper, A. E.; Tighe, T. B.; Bahnck, K. B.; Skriba, H. T.; Reinard, M. D.; Haynie, B. C.; Opila, R. L.; Winograd, N.; Allara, D. L. Bond Insertion, Complexation and Penetration Pathways of Vapor-Deposited Aluminum Atoms with HO- and CH_3O- Terminated Organic Monolayers. *J. Am. Chem. Soc.* **2002**, *124*, 5528−5541.
(46) Hooper, A.; Fisher, G. L.; Konstadinidis, K.; Jung, D.; Nguyen, H.; Opila, R.; Collins, R. W.; Winograd, N.; Allara, D. L. Chemical Effects of Methyl and Methyl Ester Groups on the Nucleation and Growth of Vapor-Deposited Aluminum Films. *J. Am. Chem. Soc.* **1999**, *121*, 8052−8064.
(47) Fisher, G. L.; Hooper, A. E.; Opila, R. L.; Allara, D. L.; Winograd, N. The Interaction of Vapor-Deposited Al Atoms with CO_2H Groups at the Surface of a Self-Assembled Alkanethiolate Monolayer on Gold. *J. Phys. Chem. B* **2000**, *104*, 3267−3273.
(48) Zhou, C.; Walker, A. V. Dependence of Patterned Binary Alkanethiolate Self-Assembled Monolayers on "UV Photopatterning" Conditions, and Evolution with Time, Terminal Group and Methylene Chain Length. *Langmuir* **2006**, *22*, 11420−11425.
(49) NIST X-ray Photoelectron Spectroscopy Database. *NIST Standard Reference Database Number 20*. National Institute of Standards and Technology: Gaithersburg MD, 2000 (retrieved Dec 2, 2018).
(50) Perry, D. L.; Taylor, J. A. X-ray photoelectron and Auger spectroscopic studies of Cu_2S and CuS. *J. Mater. Sci. Lett.* **1986**, *5*, 384−386.
(51) Biesinger, M. C. Advanced analysis of copper X-ray photoelectron spectra. *Surf. Interface Anal.* **2017**, *49*, 1325−1334.
(52) Jiang, Z.; Zhang, W.; Jin, L.; Yang, X.; Xu, F.; Zhu, J.; Huang, W. Direct XPS Evidence for Charge Transfer from a Reduced Rutile TiO2(110) Surface to Au Clusters. *J. Phys. Chem. C* **2007**, *111*, 12434−12439.
(53) Lu, P.; Shi, Z.; Walker, A. V. Selective Electroless Deposition of Copper on Organic Thin Films with Improved Morphology. *Langmuir* **2011**, *27*, 13022−13028.
(54) Lu, P.; Walker, A. V. Investigation of the Mechanism of Electroless Deposition of Copper on Functionalized Alkanethiolate Self-Assembled Monolayers Adsorbed on Gold. *Langmuir* **2007**, *23*, 12577−12582.
(55) Hedlund, J. K.; Ellsworth, A. A.; Walker, A. V. Using Surface Chemistry to Direct the Deposition of Nano-objects for Electronics. *ECS Trans.* **2018**, *86*, 89−101.
(56) Chechik, V.; Crooks, R. M.; Stirling, C. J. M. Reactions and Reactivity in Self-Assembled Monolayers. *Adv. Mater.* **2000**, *12*, 1161−1171.
(57) Martell, A. E.; Smith, R. M. *Critical Stability Constants*; Plenum Press: New York, 1974; Vol. *3*, pp 1−12.
(58) Martell, A. E.; Smith, R. M. *Critical Stability Constants*; Plenum Press: New York, 1974; Vol. *1*, pp 204−211.

https://dx.doi.org/10.1021/acs.langmuir.9b03436
Langmuir 2020, 36, 3119−3126